**Les Cahiers du GERAD** ISSN: 0711–2440

# On the frequency variation in load-flow calculations for islanded AC microgrid

M. Molénat, J. Mahseredjian, N. Rashidirad, A. Lesage-Landry

G–2024–26

March 2024



**GERAD** HEC Montréal
3000, chemin de la Côte-Sainte-Catherine
Montréal (Québec) Canada H3T 2A7

**Tél. : 514 340-6053**
Téléc. : 514 340-5665
info@gerad.ca
www.gerad.ca

# On the frequency variation in load-flow calculations for islanded AC microgrid


**Matthias Molénat** [a]

**Jean Mahseredjian** [a]

**Nasim Rashidirad** [b]

**Antoine Lesage-Landry** [a, c]

[a] *Polytechnique Montréal, Montréal (Qc), Canada, H3T 1J4*

[b] *IREQ, Hydro-Quebec, Varennes (Qc), Canada J3X 1S1*

[c] *GERAD, Montréal (Qc), Canada, H3T 1J4*

matthias.molenat@polymtl.ca
jean.mahseredjian@polymtl.ca
antoine.lesage-landry@polymtl.ca
rashidirad.nasim@hydroquebec.com



**March 2024**
**Les Cahiers du GERAD**
**G–2024–26**

**Abstract :** Load-flow analyses of islanded microgrids commonly assumes constant line admittances with respect to the grid's nominal frequency. This article analyzes errors resulting from this assumption and leverages the versatile modified-augmented-nodal analysis (MANA) formulation to propose new algorithms to account for the frequency in line admittances in load-flow calculations. The tests are implemented on an isolated 25-bus microgrid and an isolated 906-bus grid. Simulations for different loading scenarios illustrate the benefits of our approaches to the solution accuracy, especially for loadability assessment. In moderate loadability settings, the new block-dishonest Newton-Raphson method is shown to be the most efficient of the proposed algorithms. When close to the maximum loadability point, the frequency-dependent method has better performance.

**Keywords:** MANA formulation, islanded grid microgrid, droop-controlled generators, multiphase load-flow, Newton-Raphson method.

---

**Acknowledgements:** This research was supported by the multi-time-scale transients simulation for large-scale power systems chair (CRSNG, Hydro-Québec, RTE, EDF, Opal-RT) at Polytechnique Montréal. This work was firstly submitted to and accepted by the 2024 Electrimacs conference. We thank the reviewer involved in the acceptation process of this conference for their helpful advices.

# 1 Introduction

Islanded grids (IGs) and microgrids (IMGs) are gaining in popularity as distributed energy resources (DERs) become an alternative for a more sustainable power generation [9, 10]. When performing load-flow (LF) analyses in IGs and IMGs operated with, for example, droop-controlled grid-forming generators, the grid frequency $\omega$ is considered as a variable [1, 7, 8, 9, 10, 11, 12]. However, approaches based on conventional mismatch equations (CME) [1] or the modified-augmented-nodal analysis (MANA) [6, 11] using typically the Newton Raphson (NR) method [2], do not systematically account for the impact of frequency variations on line impedances. Inherited from methods for networks where the frequency is constrained to its nominal value, these approaches assume constant line impedances. Yet, frequency-dependent distribution line inductance and capacitance should affect the load-flow solution. The impacted voltages and currents, should in turn influence the droop functions of droop-controlled generators. The impact on voltage stability, for example, has been studied in [13]. Recent works [1, 7, 8, 9] introduce $\omega$ when computing the admittance matrix of the grid, $\mathbf{Y}_{\mathrm{n}}$, but uses the CME formulation which is shown to be less efficient than MANA [5, 11]. To date, the error caused by this approximation is accepted as a trade-off between LF accuracy and solvency. However, the lack of accuracy can be detrimental to the numerical resolution under critical conditions such as during loadability assessments [12, 14]. Overall, the current literature does not contain a comprehensive analysis of the impact on the accuracy of load-flow solutions when considering or not the frequency variation in line admittances.

The aim of this article is, therefore, to fill existing gaps in the literature by making the following contributions:

- We analyze the error made on voltage magnitudes induced by the frequency-independent line impedance assumption in IGs and IMGs.
- We propose improved MANA-based algorithms (`MANA-`$\mathbf{Y}(\omega)$) to account for the frequency in line admittances used in LF calculations.
- We advocate for specific approaches depending on the loading situation in order to reach better accuracy and faster convergence during LF analysis.

This paper focuses on the more efficient MANA solution method, but its conclusions on solution accuracy should be also applicable to other methods. In Section 2, we discuss errors induced when the frequency variation is omitted in line admittances. Section 3 proposes several improvements to the MANA method, whose performances are then compared in Section 4.

# 2 Frequency-dependent line admittance-based LF

Let $\mathbf{Y}(\omega) = (\mathbf{R} + j\omega\mathbf{L})^{-1}$ be the multi-phase line admittance matrix, where $\mathbf{R}$ and $\mathbf{L}$ are, respectively, the resistance and the inductance matrices. Both $\mathbf{R}$ and $\mathbf{L}$ are assumed to be constant with respect to $\omega$. Let $\mathbf{Y}_{\mathrm{n}}(\omega)$ be the matrix defining the admittance matrix of a multi-phase $n$-bus grid. We first introduce the LF analysis. We then discuss the validity of assuming $\mathbf{Y}_{\mathrm{n}}(\omega) \approx \mathbf{Y}_{\mathrm{n}}(\omega_0)$ in IGs and IMGs, where $\omega_0$ refers to the nominal frequency.

## 2.1 LF calculations for IGs and IMGs

For a given network, LF calculations consist of estimating its $m$ variables such as complex voltages and power injections and absorptions. It is done by solving a system of $m$ equations that models the load flow in the network. For a given LF formulation (e.g., MANA or CME) the LF solution is defined using a real function $F$, such as :

$$F(\mathbf{x}) = \mathbf{0}_m, \tag{1}$$

where $\mathbf{0}_m$ is the zero element of $\mathbb{R}^m$. Despite $\omega \in \mathbf{x}$, the line admittance can be assumed to be independent of $\omega$, leading to :

$$\mathbf{Y}_{\mathrm{n}}(\omega) \approx \mathbf{Y}_{\mathrm{n}}(\omega_0). \tag{2}$$

Considering the MANA framework for IMGs and IGs [11], and assuming (2) to hold, we let $F_{\mathrm{MANA}}$ be (1)'s $F$-function when the MANA formulation is used and $\mathbf{x}^*$ be the corresponding LF solution. At each iteration $j \in \mathbb{N}$, we solve the following system of Jacobian equations evaluated in $\mathbf{x}_j$:

$$\begin{bmatrix} \mathbf{Y}_{\mathrm{n}} & \mathbf{D}_{\mathrm{c}} & \mathbf{A}_{\mathrm{Ix}} & \mathbf{A}_{\mathrm{IL}} & \mathbf{A}_{\mathrm{IG}} & \mathbf{0} & \mathbf{0} \\ \mathbf{D}_{\mathrm{r}} & \mathbf{D}_{\mathrm{rc}} & \mathbf{0} & \mathbf{0} & \mathbf{0} & \mathbf{0} & \mathbf{0} \\ \mathbf{C}_{\mathrm{x}} & \mathbf{0} & \mathbf{D}_{x} & \mathbf{0} & \mathbf{0} & \mathbf{0} & \mathbf{A}_{\mathrm{x}\omega} \\ \mathbf{C}_{\mathrm{L}} & \mathbf{0} & \mathbf{0} & \mathbf{D}_{\mathrm{L}} & \mathbf{0} & \mathbf{0} & \mathbf{A}_{\mathrm{L}\omega} \\ \mathbf{C}_{\mathrm{G}} & \mathbf{0} & \mathbf{0} & \mathbf{0} & \mathbf{D}_{\mathrm{G}} & \mathbf{0} & \mathbf{A}_{\mathrm{G}\omega} \\ \mathbf{Y}_{\mathrm{G}} & \mathbf{0} & \mathbf{0} & \mathbf{0} & \mathbf{B}_{\mathrm{G}} & \mathbf{Y}_{\mathrm{GE}} & \mathbf{0} \end{bmatrix} \begin{bmatrix} \Delta\mathbf{V}_{\mathrm{n}} \\ \Delta\mathbf{I}_{\mathrm{D}} \\ \Delta\mathbf{I}_{\mathrm{x}} \\ \Delta\mathbf{I}_{\mathrm{L}} \\ \Delta\mathbf{I}_{\mathrm{G}} \\ \Delta\mathbf{E}_{\mathrm{G}} \\ \Delta\omega \end{bmatrix} = - \begin{bmatrix} \mathbf{f}_{\mathrm{n}} \\ \mathbf{f}_{\mathrm{D}} \\ \mathbf{f}_{\mathrm{x}} \\ \mathbf{f}_{\mathrm{L}} \\ \mathbf{f}_{\mathrm{G}} \\ \mathbf{f}_{\mathrm{EG}} \end{bmatrix}, \tag{3}$$

where all components of (3) are described next.

The right-hand side vector of (3) represents $-F_{\mathrm{MANA}}(\mathbf{x}_j)$ which models the network constraints. The block matrices in the Jacobian $\mathbf{J}_{F_{\mathrm{MANA}}}$ result from differentiating $F_{\mathrm{MANA}}$ and are defined in [11]. LF variables are the node voltages $\mathbf{V}_{\mathrm{n}}$, branch-dependent currents in the passive network $\mathbf{I}_{\mathrm{D}}$ and $\mathbf{I}_{\mathrm{x}}$, the load currents $\mathbf{I}_{\mathrm{L}}$, the generator currents $\mathbf{I}_{\mathrm{G}}$, the generators internal voltages $\mathbf{E}_{\mathrm{G}}$, and the frequency $\omega$. Because all these variables except for $\omega$ are complex, real and imaginary parts are split and stacked during computations. Block matrices such as $\mathbf{Y}_{\mathrm{n}}$ are represented by a two-by-two block matrix that separates real parts in the diagonal blocks and imaginary parts in the two other entries.

To account for $\omega$ in $\mathbf{Y}_{\mathrm{n}}$, we modify $\mathbf{Y}_{\mathrm{n}}$ in (1) according to the iteration frequency. We thereby introduce a MANA-$\mathbf{Y}(\omega)$ formulation, noted $F_{\text{MANA-}\mathbf{Y}(\omega)}$. We now write $\mathbf{x}^*_\omega$ to denote the solution when $F_{\text{MANA-}\mathbf{Y}(\omega)}$ is used in (1).

In the following sections, we discuss the validity of $\mathbf{x}^*$ as an approximation to $\mathbf{x}^*_\omega$.

## 2.2 NR mismatch

Using the NR method with a tolerance threshold $\epsilon_{\mathrm{tol}} > 0$, a sufficient condition to use $\mathbf{x}^*$ as an approximation for $\mathbf{x}^*_\omega$ would be $||F_{\text{MANA-}\mathbf{Y}(\omega)}(\mathbf{x}^*)||_\infty \leq \epsilon_{\mathrm{tol}}$.

To motivate further research, we test this sufficient condition solving the LF problem for the 25-bus IMG [11] and a modified 906-bus IG [3] test cases under different loading level using a linear multiplicative factor $\lambda_l > 0$. Details about the test cases are provided in the Appendix. Results are provided, respectively, in Tables 1 and 2.

In all test instances we observe that, $||F_{\text{MANA-}\mathbf{Y}(\omega)}(\mathbf{x}^*)||_\infty \gg \epsilon_{\mathrm{tol}}$. According to the NR convergence criterion, the solutions found by `MANA` do not satisfy the corresponding `MANA-`$\mathbf{Y}(\omega)$'s criterion.

**Table 1: LF calculation results and re-evaluated mismatch values for the 25-bus IMG ($f_0 = 60$ Hz and $\epsilon_{\mathrm{tol}} = 10^{-7}$).**

| $\lambda_l$ | $f$ (Hz) | $\omega$ (rad.s$^{-1}$) | $\Delta\omega/\omega_0$ (%) | $\|\|F_{\mathrm{MANA}}(\mathbf{x}^*)\|\|_\infty$ ($\times 10^{-8}$) | $\|\|F_{\text{MANA-}\mathbf{Y}(\omega)}(\mathbf{x}^*)\|\|_\infty$ |
|---|---|---|---|---|---|
| 1 | 59.80 | 375.74 | −0.33 | 4.31 | 0.39 |
| 2 | 59.59 | 374.43 | −0.68 | 2.70 | 1.67 |
| 3 | 59.37 | 373.06 | −1.04 | 2.28 | 4.02 |
| 4 | 59.13 | 371.58 | −1.43 | 3.17 | 7.73 |

**Table 2: LF calculation results and re-evaluated mismatch values for the 906-bus IG ($f_0 = 50$ Hz and $\epsilon_{\text{tol}} = 10^{-7}$).**

| $\lambda_l$ | $f$ (Hz) | $\omega$ (rad.s$^{-1}$) | $\Delta\omega/\omega_0$ (%) | $\|\|F_{\text{MANA}}(\mathbf{x}^*)\|\|_\infty$ ($\times 10^{-8}$) | $\|\|F_{\text{MANA-}\mathbf{Y}(\omega)}(\mathbf{x}^*)\|\|_\infty$ ($\times 10^{-1}$) |
|---|---|---|---|---|---|
| 1 | 49.98 | 313.05 | −0.35 | 1.12 | 0.27 |
| 2 | 49.65 | 311.93 | −0.71 | 1.12 | 1.11 |
| 3 | 49.46 | 310.75 | −1.07 | 1.49 | 2.54 |
| 4 | 49.28 | 309.62 | −1.44 | 0.93 | 4.60 |

## 2.3 Error on voltage magnitudes

In this subsection, we consider the ratio $k = X/R$ of lines in a grid, where $R$ stands for their resistance and $X$ their reactance, to discuss the error resulting from assumption (2).

For a purely resistive and inductive line of inductance $L$, assuming constant impedance implies :

$$\mathbf{Y}_{\text{n}} = \mathbf{Y}_{\text{n}}(\omega_0) \Longrightarrow k_0 = \frac{L}{R}\omega_0. \tag{4}$$

Considering $\omega$ in the line admittance, the ratio can be expressed as :

$$k = \frac{L}{R}\omega_0 + \frac{L}{R}\Delta\omega = k_0 + \Delta k. \tag{5}$$

with $\Delta k = k - k_0$ and $\Delta\omega = \omega - \omega_0$. Assuming that all droop-controlled generators inject active power to the grid, it follows that $\Delta\omega < 0$ [11]. Hence, accounting for $\omega$ when evaluating $\mathbf{Y}_{\text{n}}$ yields $k < k_0$. Consequently, the voltage value is expected to increase when considering the $\omega$-dependency on line admittance [13]. Errors on voltage magnitudes induced by Assumption (2) are also expected to increase with $\Delta\omega$.

# 3 Improved MANA algorithms

We extend the MANA approach to account for $\mathbf{Y}_{\text{n}}(\omega)$ when solving (1). In the following subsections, we propose three different constructions of a Jacobian-like $m \times m$ square matrix, thus introducing three variations of the MANA-$\mathbf{Y}(\omega)$ algorithm. We then present a hybrid approach, using a first MANA step to better initialize our proposed algorithms. A summary of the algorithm details is provided in Table 3.

## 3.1 MANA-$\mathbf{Y}(\omega)$ algorithm

Algorithm 1 proposes the formulation of a $\omega$-dependent MANA algorithm. The initial point $\mathbf{x}_0$ will be discussed in Section 3.4 and solve[equation($\boldsymbol{\gamma}$), $\boldsymbol{\gamma}$] refers to a matrix equation solver, e.g., using an LU decomposition [4], where $\boldsymbol{\gamma}$ is the unknown vector.

**Algorithm 1** MANA-$\mathbf{Y}(\omega)$.

$\mathbf{x} \leftarrow \mathbf{x}_0$
**while** $j \leq j_{\max}$ or $||F_{\text{MANA-}\mathbf{Y}(\omega)}(\mathbf{x})||_\infty \geq \epsilon_{\text{tol}}$ **do**
  $\mathbf{x} \leftarrow \mathbf{x} +$ solve $\left[\mathbf{J}_{F_{\text{MANA-}\mathbf{Y}(\omega)}}(\mathbf{x})\boldsymbol{\gamma} = F_{\text{MANA-}\mathbf{Y}(\omega)}(\mathbf{x}), \boldsymbol{\gamma}\right]$,
  $j \leftarrow j + 1$.
**end while**
**if** $||F_{\text{MANA-}\mathbf{Y}(\omega)}(\mathbf{x})||_\infty \leq \epsilon_{\text{tol}}$ **then**
  **return** $x$
**else**
  **return** Error of convergence
**end if**

Let $\mathbf{J}_{F_{\text{MANA-}\mathbf{Y}(\omega)}}$ be the Jacobian matrix of $F_{\text{MANA-}\mathbf{Y}(\omega)}$. The matrix $\mathbf{J}_{F_{\text{MANA-}\mathbf{Y}(\omega)}}$ differs from the Jacobian matrix presented in (3). First, $\mathbf{Y}_{\text{n}}$ is now substituted by $\mathbf{Y}_{\text{n}}(\omega)$ and must therefore be recalculated at each iteration. Then, new elements are added in the last column of the Jacobian to account for the derivative of $\mathbf{Y}_{\text{n}}(\omega)$ with respect to $\omega$. The differentiation of the nodal analysis equations leads to :

$$\text{d}\left[\mathbf{Y}_{\text{n}}(\omega)\mathbf{V_n}\right] = \begin{bmatrix}\mathbf{Y}_{\text{n}}(\omega) & \frac{\partial \mathbf{Y}_{\text{n}}(\omega)}{\partial \omega}\mathbf{V_n}\end{bmatrix}\begin{bmatrix}\Delta\mathbf{V_n} \\ \Delta\omega\end{bmatrix}. \tag{6}$$

The now augmented Jacobian matrix $\mathbf{J}_{F_{\text{MANA-}\mathbf{Y}(\omega)}}$ is:

$$\mathbf{J}_{F_{\text{MANA-}\mathbf{Y}(\omega)}} = \begin{bmatrix}\mathbf{Y}_{\text{n}}(\omega) & \mathbf{D}_{\text{c}} & \mathbf{A}_{\text{Ix}} & \mathbf{A}_{\text{IL}} & \mathbf{A}_{\text{IG}} & \mathbf{0} & \frac{\partial \mathbf{Y}_{\text{n}}(\omega)}{\partial \omega}\mathbf{V}_{\text{n}} \\ \mathbf{D}_{\text{r}} & \mathbf{D}_{\text{rc}} & \mathbf{0} & \mathbf{0} & \mathbf{0} & \mathbf{0} & \mathbf{0} \\ \mathbf{C}_{\text{x}} & \mathbf{0} & \mathbf{D}_{\text{x}} & \mathbf{0} & \mathbf{0} & \mathbf{0} & \mathbf{A}_{\mathbf{x}\omega} \\ \mathbf{C}_{\text{L}} & \mathbf{0} & \mathbf{0} & \mathbf{D}_{\text{L}} & \mathbf{0} & \mathbf{0} & \mathbf{A}_{\text{L}\,\omega} \\ \mathbf{C}_{\text{G}} & \mathbf{0} & \mathbf{0} & \mathbf{0} & \mathbf{D}_{\text{G}} & \mathbf{0} & \mathbf{A}_{\text{G}\omega} \\ \mathbf{Y}_{\text{G}} & \mathbf{0} & \mathbf{0} & \mathbf{0} & \mathbf{B}_{\text{G}} & \mathbf{Y}_{\text{GE}} & \mathbf{0}\end{bmatrix}. \tag{7}$$

## 3.2 BD1-MANA-$\mathbf{Y}(\omega)$ algorithm

We propose a block-wise-dishonest NR method inspired by the standard dishonest NR method [6], such that $\mathbf{J}_{F_{\text{MANA}}}$ is used as an approximation for $\mathbf{J}_{F_{\text{MANA-}\mathbf{Y}(\omega)}}$ in Algorithm 1. Benefits from a sparser and less computationally demanding matrix than the Jacobian (7) are expected.

## 3.3 BD2-MANA-$\mathbf{Y}(\omega)$ algorithm

The modification $\tilde{\mathbf{J}}_{F_{\text{MANA-}\mathbf{Y}(\omega)}}$ of $\mathbf{J}_{F_{\text{MANA-}\mathbf{Y}(\omega)}}$ is defined as :

$$\tilde{\mathbf{J}}_{F_{\text{MANA-}\mathbf{Y}(\omega)}} = \begin{bmatrix}\mathbf{Y}_{\text{n}}(\omega) & \mathbf{D}_{\text{c}} & \mathbf{A}_{\text{Ix}} & \mathbf{A}_{\text{IL}} & \mathbf{A}_{\text{IG}} & \mathbf{0} & \mathbf{0} \\ \mathbf{D}_{\text{r}} & \mathbf{D}_{\text{rc}} & \mathbf{0} & \mathbf{0} & \mathbf{0} & \mathbf{0} & \mathbf{0} \\ \mathbf{C}_{\text{x}} & \mathbf{0} & \mathbf{D}_{\text{x}} & \mathbf{0} & \mathbf{0} & \mathbf{0} & \mathbf{A}_{\mathbf{x}\omega} \\ \mathbf{C}_{\text{L}} & \mathbf{0} & \mathbf{0} & \mathbf{D}_{\text{L}} & \mathbf{0} & \mathbf{0} & \mathbf{A}_{\text{L}\,\omega} \\ \mathbf{C}_{\text{G}} & \mathbf{0} & \mathbf{0} & \mathbf{0} & \mathbf{D}_{\text{G}} & \mathbf{0} & \mathbf{A}_{\text{G}\omega} \\ \mathbf{Y}_{\text{G}} & \mathbf{0} & \mathbf{0} & \mathbf{0} & \mathbf{B}_{\text{G}} & \mathbf{Y}_{\text{GE}} & \mathbf{0}\end{bmatrix}. \tag{8}$$

In this case, we omit the block-matrix $\frac{\partial \mathbf{Y}_{\text{n}}(\omega)}{\partial \omega}\mathbf{V_n}$ in order to work with a more accurate but less computationally demanding matrix than the full $\mathbf{J}_{F_{\text{MANA-}\mathbf{Y}(\omega)}}$. Using $\tilde{\mathbf{J}}_{F_{\text{MANA-}\mathbf{Y}(\omega)}}$ as an approximation for $\mathbf{J}_{F_{\text{MANA-}\mathbf{Y}(\omega)}}$ in Algorithm 1 is a compromise between the two previous approaches.

## 3.4 Initialization and hybrid algorithms

Algorithm 1 is initialized with $\mathbf{x}_0$, an estimated value of $\mathbf{x}^*_\omega$. The choice of the initial point has a direct impact on the convergence of the NR method. Several initialization procedures emerge from the literature, e.g., flat-start or MANA-initialized. We opt for a MANA-initialized initial point because it has been shown to perform better than other methods in [11].

We propose in Algorithm 2 a hybrid version of Algorithm 1. The first step from line 1 to line 5 is based on the `MANA` algorithm and Assumption (2). We then propose a second step based on the `MANA-`$\mathbf{Y}(\omega)$ algorithm with $\mathbf{x}^*$ as a new initial point, defining the `h-MANA-`$\mathbf{Y}(\omega)$ approach. We analogly define the `h-BD1-MANA-`$\mathbf{Y}(\omega)$ and `BD2-MANA-` $\mathbf{Y}(\omega)$ approaches. The first step is expected to provide a better initial point for the second part of the algorithm, thus reducing the number of iterations for convergence of approaches presented with Algorithm 1.

**Algorithm 2** `h-MANA-`$\mathbf{Y}(\omega)$.

$\mathbf{x} \leftarrow \mathbf{x}_0$
**while** $j \leq j_{\max}$ or $||F(\mathbf{x})||_\infty \geq \epsilon_{\text{tol}}$ **do**
  $\mathbf{x} \leftarrow \mathbf{x} +$ `solve` $\left[\mathbf{J}_{F_{\text{MANA}}}(\mathbf{x})\boldsymbol{\gamma} = F_{\text{MANA}}(\mathbf{x}), \boldsymbol{\gamma}\right]$
  $j \leftarrow j + 1$
**end while**
**if** $j = j_{\max}$ **then**
  **return** Error of convergence
**else**
  use `MANA-`$\mathbf{Y}(\omega)$ with $\mathbf{x}_0 \leftarrow \mathbf{x}$
**end if**

**Table 3: Comparison of the different MANA-based algorithms.**

| Method | `MANA` [11] | `MANA-`$\mathbf{Y}(\omega)$ | `BD1-MANA-`$\mathbf{Y}(\omega)$ | `BD2-MANA-`$\mathbf{Y}(\omega)$ |
|---|---|---|---|---|
| $\mathbf{x}_0$ | MANA-init. | MANA-init. | MANA-init. | MANA-init. |
| $F$ | $F_{\text{MANA}}$ | $F_{\text{MANA-}\mathbf{Y}(\omega)}$ | $F_{\text{MANA-}\mathbf{Y}(\omega)}$ | $F_{\text{MANA-}\mathbf{Y}(\omega)}$ |
| $\mathbf{J}$ | $\mathbf{J}_{F_{\text{MANA}}}$ (3) | $\mathbf{J}_{F_{\text{MANA-}\mathbf{Y}(\omega)}}$ (7) | $\mathbf{J}_{F_{\text{MANA}}}$ (3) | $\tilde{\mathbf{J}}_{F_{\text{MANA-}\mathbf{Y}(\omega)}}$ (8) |
| Results | $\mathbf{x}^*$ | $\mathbf{x}^*_\omega$ | $\mathbf{x}^*_\omega$ | $\mathbf{x}^*_\omega$ |

| Method | `h-MANA-`$\mathbf{Y}(\omega)$ | `h-BD1-MANA-`$\mathbf{Y}(\omega)$ | `h-BD2-MANA-`$\mathbf{Y}(\omega)$ |
|---|---|---|---|
| $\mathbf{x}_0$ | $\mathbf{x}^*$ (from `MANA`) | $\mathbf{x}^*$ (from `MANA`) | $\mathbf{x}^*$ (from `MANA`) |
| $F$ | $F_{\text{MANA-}\mathbf{Y}(\omega)}$ | $F_{\text{MANA-}\mathbf{Y}(\omega)}$ | $F_{\text{MANA-}\mathbf{Y}(\omega)}$ |
| $\mathbf{J}$ | $\mathbf{J}_{F_{\text{MANA-}\mathbf{Y}(\omega)}}$ (7) | $\mathbf{J}_{F_{\text{MANA}}}$ (3) | $\tilde{\mathbf{J}}_{F_{\text{MANA-}\mathbf{Y}(\omega)}}$ (8) |
| Results | $\mathbf{x}^*_\omega$ | $\mathbf{x}^*_\omega$ | $\mathbf{x}^*_\omega$ |

# 4 Numerical study

In this section, we discuss the solution quality and the convergence properties of the MANA-$\mathbf{Y}(\omega)$ methods. Tests are performed on a 25-bus IMG [11] and a modified 906-bus IG [3] under different loading levels $\lambda_l$. Each generator is not subject to a maximum power constraint. Implementation is done in MATLAB and executed on an i7, CPU 2.8 GHz, with 16.0 GB of memory. Computation times are averaged on 20 identical runs.

## 4.1 Solution quality

We run `MANA` and our proposed approaches on the 25-bus IMG and a 906-bus IG test cases under loading level $\lambda_l \in [\![1, 7]\!]$. Frequency values and voltage magnitudes at selected buses are provided in Table 4.

We observe that, as expected from Section 2.3, voltage magnitudes in $\mathbf{x}^*_\omega$ are greater than in $\mathbf{x}^*$. Yet, $\omega \in \mathbf{x}^*_\omega$ and $\omega \in \mathbf{x}^*$ remains consistent and their difference is negligible in comparison to $|\omega - \omega_0|$. As grids experience overloading, we notice a marginal increase in the frequency error. Despite this, the error on the generator voltage remains minor as seen with voltage magnitudes at bus 13 for the 25-bus IMG and at bus 400 for the 906-bus. We consider the 25-bus IMG under an extreme loading ($\lambda_l = 7.47$, empirically observed to be close to the maximum loadability point). The maximum absolute relative error at each node for voltage magnitudes in $\mathbf{x}^*$ in comparison to in $\mathbf{x}^*_\omega$ is presented in Figure 1. In this case, Assumption (2) leads to an increasing error on voltage magnitudes as we get further downstream of a source. For example, Assumption (2) yields a relative error of over 5% for voltage values at bus 15, one of the buses furthest away from the generators.

## 4.2 Convergence studies

We now compare the average computation time and required number of iterations of our approaches : `MANA-`$\mathbf{Y}(\omega)$, `BD1-` MANA-$\mathbf{Y}(\omega)$, `BD2-MANA-`$\mathbf{Y}(\omega)$, and their hybrid versions. We run the LF analysis for the 25 bus IMG and the 906-bus IG under several loading condition $\lambda_l$ below the maximum loadability point. We collect the results in Figures 2 and 3. The outcome of the first MANA step

**Table 4: LF calculations for the 25-IMG and 906-bus IG under different loading level $\lambda_l$. Voltage magnitudes are in V, $\omega$ in rad.s$^{-1}$.**

| **25-bus** | $\lambda_l = 1$ | | | | **906-bus** | $\lambda_l = 1$ | | | |
|---|---|---|---|---|---|---|---|---|---|
| | $\omega$ | $\lvert\mathbf{V}_{1,a}\rvert$ | $\lvert\mathbf{V}_{8,a}\rvert$ | $\lvert\mathbf{V}_{13,a}\rvert$ | | $\omega$ | $\lvert\mathbf{V}_{1,a}\rvert$ | $\lvert\mathbf{V}_{400,a}\rvert$ | $\lvert\mathbf{V}_{600,a}\rvert$ |
| $\mathbf{x}^*$ | 375.74 | 2331.1 | 2317.8 | 2380.5 | | 313.05 | 238.47 | 239.28 | 238.92 |
| $\mathbf{x}^*_\omega$ | 375.74 | 2331.2 | 2317.9 | 2380.5 | | 313.05 | 238.47 | 239.28 | 238.92 |
| **25-bus** | $\lambda_l = 4$ | | | | **906-bus** | $\lambda_l = 4$ | | | |
| | $\omega$ | $\lvert\mathbf{V}_{1,a}\rvert$ | $\lvert\mathbf{V}_{8,a}\rvert$ | $\lvert\mathbf{V}_{13,a}\rvert$ | | $\omega$ | $\lvert\mathbf{V}_{1,a}\rvert$ | $\lvert\mathbf{V}_{400,a}\rvert$ | $\lvert\mathbf{V}_{600,a}\rvert$ |
| $\mathbf{x}^*$ | 371.58 | 2085.2 | 2023.4 | 2309.5 | | 309.61 | 233.18 | 236.51 | 235.02 |
| $\mathbf{x}^*_\omega$ | 371.58 | 2086.7 | 2025.3 | 2309.6 | | 309.61 | 233.19 | 236.51 | 235.03 |
| **25-bus** | $\lambda_l = 7$ | | | | **906-bus** | $\lambda_l = 7$ | | | |
| | $\omega$ | $\lvert\mathbf{V}_{1,a}\rvert$ | $\lvert\mathbf{V}_{8,a}\rvert$ | $\lvert\mathbf{V}_{13,a}\rvert$ | | $\omega$ | $\lvert\mathbf{V}_{1,a}\rvert$ | $\lvert\mathbf{V}_{400,a}\rvert$ | $\lvert\mathbf{V}_{600,a}\rvert$ |
| $\mathbf{x}^*$ | 365.73 | 1701.3 | 1550.8 | 2208.2 | | 305.97 | 227.61 | 233.60 | 230.94 |
| $\mathbf{x}^*_\omega$ | 365.78 | 1714.6 | 1567.8 | 2210.3 | | 305.96 | 227.62 | 233.60 | 230.95 |

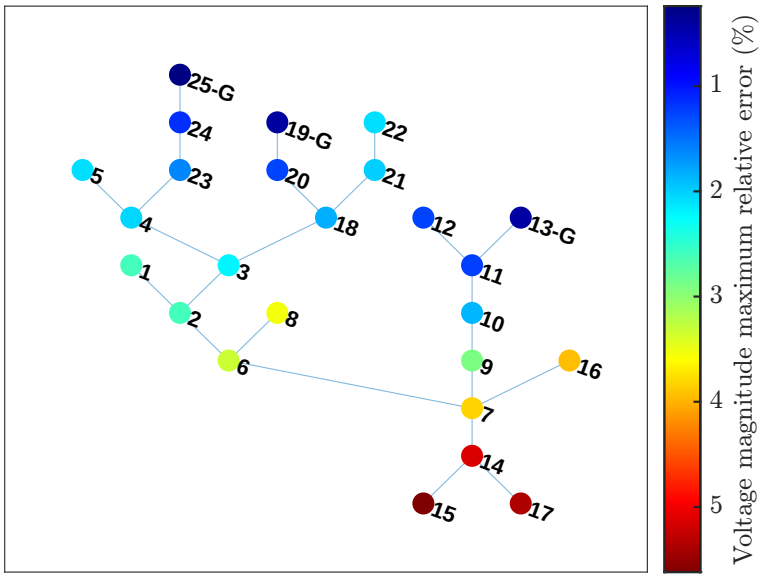


**Figure 1: Maximum relative difference between MANA's and MANA-$\mathbf{Y}(\omega)$'s voltage magnitudes for a 25-bus IMG droop-controlled generators (G) and loading level of $\lambda_l = 7.47$.**

for hybrid algorithms is considered as given, to focus on the effects of proposed initialization over the MANA-$\mathbf{Y}(\omega)$ performance. The overall MANA-$\mathbf{Y}(\omega)$ performance of hybrid approaches can be extrapolated by combining the MANA and MANA-$\mathbf{Y}(\omega)$ steps in Figures 2 and 3.

All MANA-$\mathbf{Y}(\omega)$ based LF calculations require more iterations to reach convergence than `MANA`. From one variant of `MANA`-$\mathbf{Y}(\omega)$ to another, the number of iterations needed increases with the level of approximation made on the Jacobian matrix. Considering the computation time, more complex matrices, e.g., denser or with more iteration-dependent entries affects each iteration. As such, creation and inversion of matrices in our approaches take more time than the standard MANA method, resulting in an overall slow down.

When MANA-$\mathbf{Y}(\omega)$ based LF calculations is employed following an initialization done with `MANA` and Assumption (2), the number of iteration is reduced in comparison to regular MANA-$\mathbf{Y}(\omega)$ approaches. The benefit of hybridization when including computation from the `MANA` step becomes clear when considering large IGs such as the 906-bus IG. While more iterations are needed overall, the slight reduction in time-consuming `MANA`-$\mathbf{Y}(\omega)$ iterations can lead to a shorter computation time than the corresponding method without hybridization.

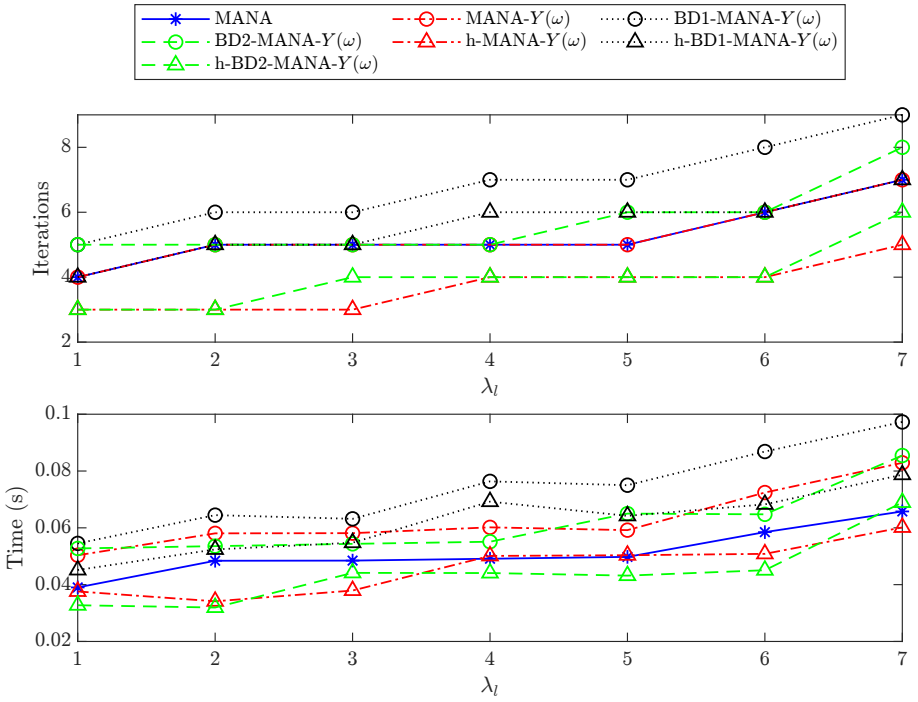


**Figure 2: Algorithm performance for LF calculation in the case of a 25-bus IMG under various loading condition $\lambda_l$. Notes: For hybrid algorithms (`h-`), the `MANA` step computations are not included.**

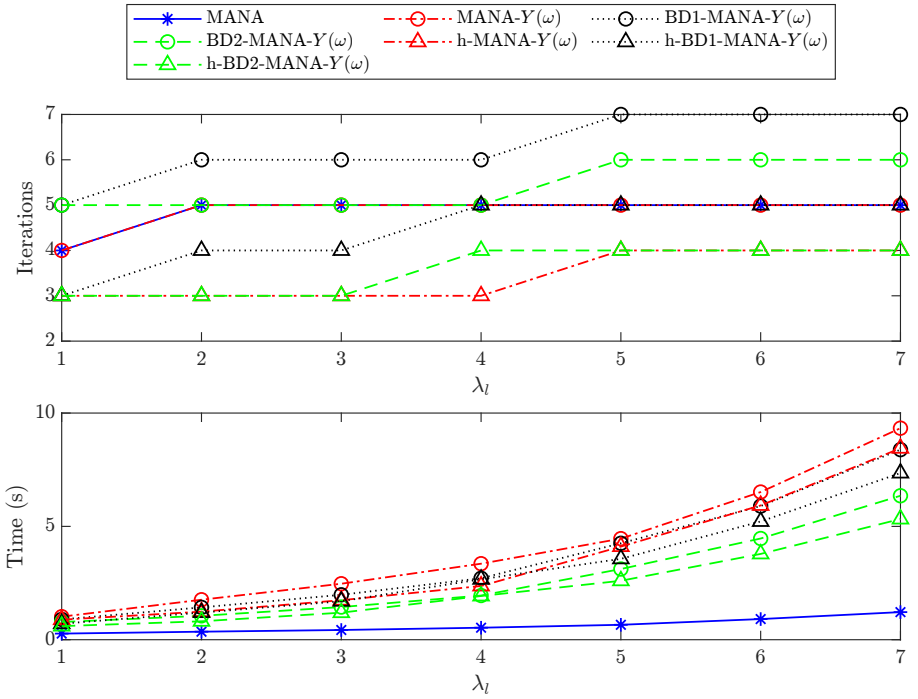


**Figure 3: Algorithm performance for LF calculation in the case of a 906-bus IG under various loading condition $\lambda_l$. Notes: For hybrid algorithms (`h-`), the `MANA` step computations are not included.**

LF calculations are numerically unstable when the grid is close to its maximum loadability point, as illustrated in Figure 4. Assumption (2) leads to (1) having no numerical solution for high values of $\lambda_l$: it has then virtually collapsed. Although `MANA` diverges, `MANA-`$\mathbf{Y}(\omega)$ converges past this apparent

maximum loadability point. At high loading, approximations have significant impacts on algorithm performance. Consequently, hybrid methods reach the same limit as the standard MANA method : Assumption (2) in Algorithm 2's first step leads to divergence for lower $\lambda_l$ than algorithms based on Algorithm 1.

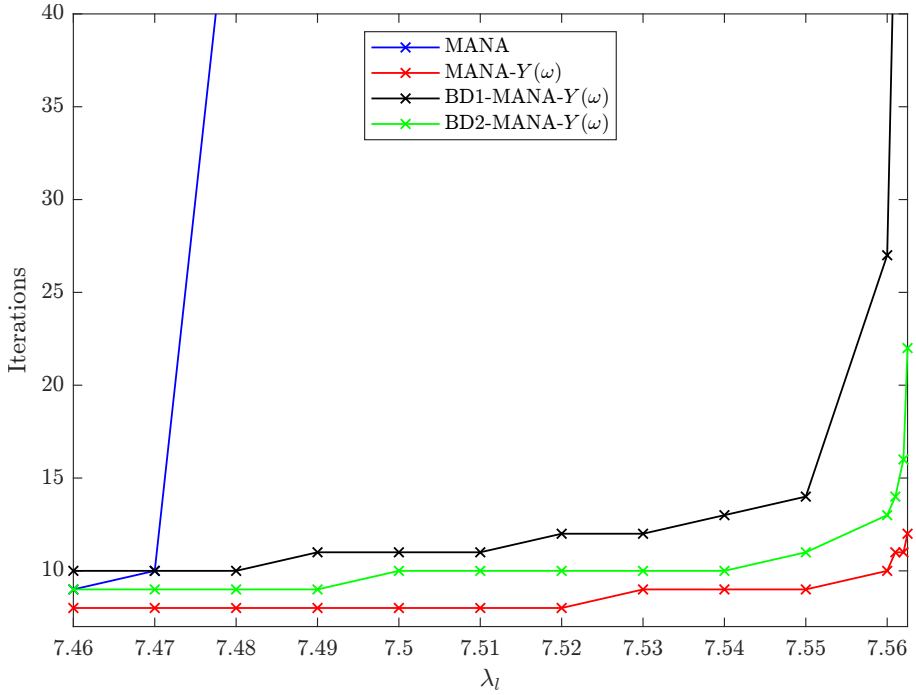


**Figure 4: Algorithm performance for the heavily loaded 25-bus IMG.**

In heavy overloading instances, it is therefore preferred to use the full `MANA-`$\mathbf{Y}(\omega)$ algorithm. Globally, `BD2-MANA-` $\mathbf{Y}(\omega)$ strikes a good balance in terms of accuracy, time computation, and numerical stability.

# 5 Conclusion

Assuming frequency-independent line admittances in purely resistive and inductive islanded grids results in the under-evaluation of voltages when solving the LF problem. Experimentations provide insights on the impacts of the grid characteristics on errors made by the LF formulation (1). To address this issue, a frequency-dependent admittance-based formulation is considered. We define several NR-based methods to solve this formulation.

Our numerical tests verify the advantages of our methods and we draw comparisons between them. Using $\mathbf{J}_{F_{\text{MANA-}\mathbf{Y}(\omega)}}$, we lose one of the main computational advantages of the standard MANA method: at each iteration, a larger number of entries has to be updated. In both block-dishonest methods, we try to retain this advantage, but we require more iteration to converge due to approximations. Hybrid methods try to benefit from an improved initial point using `MANA` in order to speed up the new methods. However, these hybrid methods inherits its limitation in extreme loading cases. The choice of one of these algorithms will result from balancing the trade-off between number of iterations, resolution speed, and accuracy.

# Appendix

**Grid details :** Grid details are given in Table 5.

**Table 5: Grid generation information.**

| Grid | $n^\circ$ bus | type | $V_{nom}$ (kV) | $\alpha$ ($\times 10^4$) | $\beta$ ($\times 10^4$) | $S_{gen}$ (kW) | $f_{nom}$ (Hz) |
|---|---|---|---|---|---|---|---|
| **25-bus IMG** | 13 | Synch. | 4.16 | 106 | 5.00 | 4000 | 60 |
| | 19 | Inv. | 4.16 | 53.1 | 2.50 | 2000 | 60 |
| | 25 | Inv. | 4.16 | 106 | 5.00 | 4000 | 60 |
| **906-bus IG** | 400 | Synch. | .416 | 3.18 | 20.6 | 1000 | 50 |
| | 800 | Synch. | .416 | 1.59 | 10.3 | 500 | 50 |

# References


[1] M.A. Allam, A.A. Hamad, and M. Kazerani. A generic modeling and power-flow analysis approach for isochronous and droop-controlled microgrids. IEEE Transactions on Power Systems, 33(5):5657–70, 2018.

[2] S. Bhowmick. Flexible AC Transmission Systems (FACTS): Newton Power-Flow Modeling of Voltage-Sourced Converter-Based Controllers. CRC Press, 2018.

[3] IEEE PES Test FEeder. The ieee european low voltage test feeder, 2015.

[4] R. A. Horn and C. R. Johnson. Matrix analysis. Cambridge university press, 2012.

[5] Z. Javid, T. Xue, U. Karaagac, and I. Kocar. Unified power flow solver for hybrid ac/dc distribution networks. IEEE Transactions on Power Delivery, pages 1–11, 2023.

[6] I. Kocar, J. Mahseredjian, U. Karaagac, G. Soykan, and O. Saad. Multiphase load-flow solution for large-scale distribution systems using mana. IEEE Transactions on Power Delivery, 29(2):908–915, 2014.

[7] A. Lima-Silva, F. D. Freitas, and L. F. de J. Fernandes. A homotopy-based approach to solve the power flow problem in islanded microgrid with droop-controlled distributed generation units. Energies, 16(14), 2023.

[8] A. H. Lone and Neeraj G. A novel modified decoupled newton-raphson load flow method with distributed slack bus for islanded microgrids considering frequency variations. Electric Power Components and Systems, 52(5):678–696, 2024.

[9] F. Mumtaz, M. H. Syed, M. Al Hosani, and H. H. Zeineldin. A novel approach to solve power flow for islanded microgrids using modified newton raphson with droop control of dg. IEEE Transactions on Sustainable Energy, 7(2):493–503, 2016.

[10] D. E. Olivares, A. Mehrizi-Sani, A. H. Etemadi, C. A. Cañizares, R. Iravani, M. Kazera ni, A. H. Hajimiragha, O. Gomis-Bellmunt, M. Saeedifard, R. Palma-Behnke, G. A. Jiménez-Esté vez, and N. D. Hatziargyriou. Trends in microgrid control. IEEE Transactions on Smart Grid, 5(4):1905–1919, 2014.

[11] N. Rashidirad, J. Mahseredjian, I. Kocar, U. Karaagac, and O. Saad. Mana-based load-flow solution for islanded ac microgrids. IEEE Transactions on Smart Grid, 2022.

[12] N. Rashidirad, J. Mahseredjian, I. Kocar, S. M. Mohseni-Bonab, and O. Saad. Loadability assessment of droop-controlled islanded microgrids: Integration of droop control functions under unbalanced loading. In IECON 2023- 49th Annual Conference of the IEEE Industrial Electronics Society, pages 1–6, 2023.

[13] M. Shukla and A. Sekar. Study of the effect of x/r ratio of lines on voltage stability. In Proceedings of the 35th Southeastern Symposium on System Theory, 2003., pages 93–97, 2003.

[14] X. Xu, Z. Yan, M. Shahidehpour, S. Chen, H. Wang, Z. Li, and Q. Zhou. Maximum loadability of islanded microgrids with renewable energy generation. IEEE Transactions on Smart Grid, 10(5):4696–4705, 2019.